Supplementary Materials for

An ingestible self-orienting system for oral delivery of macromolecules

Alex Abramson, Ester Caffarel-Salvador, Minsoo Khang, David Dellal, David Silverstein, Yuan Gao, Morten Revsgaard Frederiksen, Andreas Vegge, František Hubálek, Jorrit J. Water, Anders V. Friderichsen, Johannes Fels, Rikke Kaae Kirk, Cody Cleveland, Joy Collins, Siddartha Tamang, Alison Hayward, Tomas Landh, Stephen T. Buckley, Niclas Roxhed, Ulrik Rahbek, Robert Langer*, Giovanni Traverso*

*Corresponding author. Email: rlanger@mit.edu (R.L.); ctraverso@bwh.harvard.edu (G.T.)

Published 8 February 2019, *Science* **363**, 611 (2019)
DOI: 10.1126/science.aau2277

This PDF file includes:

Materials and Methods
Supplementary Text
Figs. S1 to S16
Tables S1 to S3
Caption for Movie S1
References

Other Supplementary Material for this manuscript includes the following:
(available at www.sciencemag.org/content/363/6427/611/suppl/DC1)

Movie S1 (.mov)
MATLAB Code (.zip)

Materials and Methods

Dulbecco's Phosphate-Buffered Saline (PBS) was purchased from Gibco by Life Technologies (Woburn, USA). Human insulin was obtained from Novo Nordisk (Maalov, Denmark). 200,000 molecular weight PEO, 45,000 molecular weight Polycaprolactone (PCL), and sucrose was purchased from Sigma Aldrich (Saint Louis, USA). 301 steel springs were custom fabricated by Madsens Fjedrefabrik (Brondby, Denmark). The three custom fabricated springs possessed the specifications show in Table S3. The 1.7 N spring was purchased from Lee Spring Company (Brooklyn, USA) and is serial #CI008B05S316. Isomalt was purchased from CK Products (Fort Wayne, USA). Elastosil M 4642 B was obtained from Wacker Chemie AG (Munich, Germany).

Device fabrication:

A two part negative mold was designed in Solidworks (Dassault Systemes, Velizy-Villacoublay, France) and printed on a Form 2 3D printer (Formlabs, Somerville, USA) for the Ellipsoid, Sphere and SOMA top portions. Each device was designed to have a weight of 0.77 g with 88% of the weight comprised of stainless steel and the resulting weight comprised of PCL. The PCL top portions were cast into the negative mold in a melted state to form the top section of the device, and the bottom part was created from 316L stainless steel using a milling machine and fabricated by Novo Nordisk's Device Department.

The springs were then fixed to the top section of the device using melted PCL, and the drug loaded millipost was attached to the spring again using PCL. Finally, the devices were attached together using PCL.

Before creating the stainless-steel parts, prototype models were made with Field's metal purchased from Alfa Aesar (Haverville, USA). The low melting point of this metal alloy allows for easy device fabrication, and its 7.88 g/cm^3 density is similar to that of stainless steel (7.7g/cm^3). These prototypes were used to assess the device in vitro and ex vivo. Stainless steel and PCL devices were used in all in vivo experiments, and were also used in experiments measuring the SOMA's orientation ability in air and water, inside of an excised stomach, and in the presence of motion.

Spring Actuator fabrication:

Hardened isomalt and sucrose were used to hold the spring in compression. Sucrose or isomalt was melted by heating it to 210°C for 15 minutes and molded inside a SYLGARD 184 Elastomer Kit (Dow Chemical, Midland, USA). When molded, this material could then be used as a barrier or an encapsulation to hold the spring in compression. To encapsulate the spring inside of the material, a spring was placed inside the mold filled with molten material and heated for an additional 5 minutes in the oven (Fig. S14). The mold was removed from the oven, and a tailor-made plunger was used to compress the spring into the material. The encapsulated spring was then left to cool before being removed from the mold.

Insulin millipost fabrication

Insulin milliposts were fabricated as described in the paper and in Fig. 3a.

SOMA Membrane fabrication

Membranes were cast from a custom made aluminum mold and fabricated from Elastosil M 4642 B. Membrane valves were cut using a custom made razor blade punch. The membranes were

placed into the SOMA devices as shown in Fig. S12. Each membrane was 100 μm thick. Penetration friction forces were tested by fixing milliposts to an Instron 5943 (Instron, Norwood, USA) and reading the force measurements using a 10 N load cell (Instron) as the milliposts were propelled through the valve at 1 mm/s.

Self-orienting experiments in various fluids

To calculate the righting speeds of the devices, we used a Vision Research Phantom v7.1 monochrome high-speed-video camera (Vision Research, Homewood, USA) recording at 1000 fps. SOMAs made from PCL and Field's metal as well as PCL and 316L stainless steel were released from a 30°, 90°, or 135° angle while submerged inside of a 2 x 5 x 10 cm^3 clear plastic vessel in one of the following fluids: air, canola oil (Crisco, Orrville, USA); gastric fluid obtained from a Yorkshire swine and filtered using a 10 μm syringe filter; reconstituted mucin from porcine stomach at 10 mg/mL in 1 M NaOH (Sigma-Aldrich, St. Louis, USA); and tap water (Cambridge, USA). A line was drawn on the axial plane of the device in order to determine the angle in a given frame, and orientation speeds were determined using sequential image analysis in Image J (Open Source). A device was considered oriented when the line drawn was perpendicular to the bottom of the vessel.

SOMA self-orientation in a food particle bath was performed by combining 4 ounces roast beef, a 2 ounce dinner roll, and 2 ounces of cooked spinach prepared by Aramark at the Koch Café (Cambridge, USA) with 8 fluid ounces of water. The materials were blended for 30 seconds on high in a Ninja 1000W blender (SharkNinja Operating LLC, Needham, USA) and poured into a 4 cm in diameter container up to a height of 20 cm. SOMA devices were then dropped into the mixture and imaged after they reached the bottom to determine their orientation.

Self-Orienting Experiments in Excised Swine Stomach

Swine tissue for ex vivo evaluation was acquired from the Blood Farm Slaughterhouse (West Groton, USA). Swine were euthanized, and fresh tissue was procured and stored on ice. Tissue was tested within 6 hours of euthanasia. To determine the orienting efficiency of devices in a stomach, an intact Yorkshire swine stomach was positioned to hang so that the esophageal sphincter and the pyloric sphincter were elevated above the body of the stomach. A 12.7 cm long and 1.9 cm diameter Tygon tube was then inserted into and clamped against the esophageal sphincter of the stomach to mimic the esophagus. The stomach was then filled with water, and devices were dropped through the tube and into the stomach. Through a window cut on the uppermost section of the stomach (lesser curvature), devices were assessed to determine whether or not the desired side of the device was in contact with the tissue wall. This experiment was performed with SOMA shapes made with just PCL as well as SOMA shapes made with Field's metal and PCL, as well as 316L stainless steel and PCL. Additionally the ellipsoid and the sphere devices were tested as well.

Resistance to outside motion testing

Resistance to outside motion was tested in vitro by submerging devices in water inside of a 500 mL Erlenmeyer flask and recording them while on a tilting shaker using a 15° tilt at 50 rpm. Footage was assessed using Image J on a frame by frame basis and the tilting angle was calculated by determining the maximum angle between the axial plane of the device and the plane of the shaker table over one tilt period.

In vivo simulated walking test

All animal experiments were approved by and performed in accordance with the Committee on Animal Care at MIT. Female Yorkshire swine were obtained from Tufts University (Medford, USA) for in vivo experiments. Swine sedation was performed as described below in the "in vivo insulin delivery evaluation" section. Two devices were fed to a swine using an overtube. One device was a SOMA, while another device was of the same shapes as an SOMA but made entirely out of PCL containing a steel washer for X-ray visualization purposes. The swine was moved rostro-caudally and laterally as well as rolled from left lateral side to right lateral side two times. Next the swine was placed back on the table and rolled 180 degrees. Finally, an X-ray was taken to visualize the orientation of the devices. These X-rays were compared to in vitro X-rays where the devices were placed at known angles. Since the stomach of a swine contains different curvatures, a device was considered oriented if it was within 30 degrees of the perpendicular plane of the X-ray (Fig. S2).

Micro Computed Tomography and Barium Sulfate millipost fabrication

A SOMA device loaded with a barium sulfate millipost was actuated by dripping 37°C water onto the device. The SOMA was actuated on top of ex vivo swine stomach tissue placed in a 60 mm diameter disposable petri dish (VWR, Radnor, USA). After actuation, the device and tissue were transferred to a GE CT120 microCT imaging system (General Electric, Boston, USA) for imaging. Barium sulfate milliposts were as described in the paper and in Fig. 3a with one change. Instead of concentrating the barium sulfate at the tip portion, the entire millipost contained 20% barium sulfate.

Needle penetration force testing in vivo

We constructed a specialized stage to test force insertion profiles in vivo (Fig. S7). This device consisted of a motor that moved an arm downwards towards a piece of tissue at a controlled speed of 0.2 mm/s. We placed a force gauge and a camera on the moving stage. As the needle penetrated the tissue, the force and movie measurements along with the video feed were recorded in LabVIEW (National Instruments, Austin, USA). Yorkshire swine were sedated as described in the "In vivo Insulin Delivery Evaluation" methods section. A laparotomy procedure was performed to access the gastric surface mucosa. Gastric tissue was reflected to reveal a working area of at least 7.5 x 7.5 cm^2. The custom apparatus was then positioned above the tissue and used to insert the milliposts at 0.2 mm/s. Intraoperative measurements were affected by breathing and we determined that the displacement caused by breathing accounted for an extra 3 mm of insertion. This was measured using a ruler and confirmed by comparing the forces on the needles during inhalation and exhalation during the entire insertion process. It was seen that the forces read during exhaled state equaled the forces felt during the inhaled state 3 mm earlier. In vivo force measurements were read by a 10 N force gauge (Shimpo, Cedarhurst USA) with an accuracy of ±0.03 N and a resolution of 0.01 N.

Insulin millipost in vitro dissolution

Three 50 ml-Falcon tubes were filled with 2 mL of PBS and incubated at 37±0.1°C. At the beginning of the test, one insulin millipost tip was submerged in each of the Falcon tubes. A rack containing the tubes was placed in an Innova 44 Shaker Series incubator (New Brunswick Scientific, Edison, USA) set to 37±0.1°C and 50 rpm.

The tubes were sampled every three minutes until 15 minutes elapsed and then every 5 minutes until 60 minutes elapsed. At each of these times, the test tube rack was removed from the incubator and 200 μL of solution was pipetted into an HPLC vial. Then, 200 μL of PBS at 37±0.1°C was pipetted back into the tubes. The test tube rack was reinserted into the incubator. A blank reference sample was also collected from a vial of pure PBS incubated at 37±0.1°C. The HPLC vials were tested in an HPLC machine (Agilent, Santa Clara, USA) to determine the amount of dissolved insulin at a given time using a method retrieved from the following paper (40) with a modification to the run time. Briefly, we utilized a 7.8 x 300 mm^2 Insulin HMWP column (Waters Corp, Milford, USA) set to room temperature. We performed the elution with a flow rate of 0.5 mL/min for 26 minutes using a mobile phase made from 15% acetic acid (v/v), 20% acetonitrile (v/v), and 0.65 g/L L-arginine all purchased from (Sigma-Aldrich).

Insulin stability testing

Insulin millipost tips were placed inside of a desiccated pill container and left inside of a climate controlled room set to 40°C and 75% relative humidity. An identical batch of millipost tips was placed inside of a climate controlled chamber at 5°C and 15% relative humidity. Additionally, a liquid formulation of pure insulin dissolved in PBS at a concentration of 4 mg/mL was placed inside of the two climate chambers as well. The samples were left for 0, 2, 4, and 16 weeks. Once removed, dissolution tests were performed on the milliposts in addition to a high molecular weight protein (HMWP) analysis, activity testing, and a Raman spectroscopy analysis. The Raman analysis is described in a later section entitled "Raman Spectroscopy", while the HMWP analysis was performed using the HPLC method described in the "in vitro dissolution" section, and the activity testing was performed using a receptor binding assay developed by Novo Nordisk described elsewhere (41, 42). In a few words, a scintillation proximity assay (SPA) was performed on the human insulin from the millipost, and the binding receptor affinities were verified by competition of the human insulin from the millipost and [125I]TyrA14-labeled insulin (Novo Nordisk) in the SPA. We analyzed the affinities using a four-parameter logistic model and compared the results to untreated human insulin.

Raman spectroscopy

A DXRxi EM-CCD Raman Imaging microscope (ThermoFisher Scientific, Waltham, USA), was used to image the insulin and PEO compressed mixtures. Samples were exposed to a laser wavelength of 780 nm at a power of 24 mW and a frequency of 200 Hz. The laser beam was focused through a 20x NA 0.40 objective and the scattering collected through same. Rayleigh and anti-Stokes scattering were blocked by an edge filter prior to entrance to a spectrograph configured with a 400 line/mm grating. Areas of 200x200 μm^2 were scanned with a scanning step size of 5 μm in each dimension. 300 scans of each section were taken. In order to smooth the data, a principal component analysis was performed to eliminate spectrums with high noise, and a root mean squared analysis was performed to further filter the data. To ensure that we did not cut out only sections with a high percentage of PEO or insulin, we compared the extracted points with their neighboring sections to ensure that entire sections of the sample were not being removed. We used MATLAB's peak finding tools to determine the peak location and width of the peaks of interest. Only insulin peaks which did not overlap with the PEO peaks were analyzed, and the results are detailed in Fig. S3. Peaks are identified using the following reference (43).

Enzyme activity assays

We fabricated millipost tips as described above, however, instead of using insulin as an active ingredient, we used lysozyme from chicken egg (Sigma Aldrich) and glucose-6-phosphate dehydrogenase expressed in E. coli (G6PD) as the API (Sigma Aldrich). To perform the activity assay on G6PD, we used an activity assay kit (Sigma Aldrich) which measures the amount of oxidized glucose-6-phosphate. Protein mass was calculated using a Bicinchoninic Acid Kit for protein determination (Sigma Aldrich). We fabricated 3 millipost tips using 40% G6PD and 60% PEO 200k and dissolved them all together to perform the assay. We then compared this to G6PD that was not compressed into a millipost tip.

To measure the activity of lysozyme, we used the assay provided by Sigma Aldrich which measures the amount of lysed Micrococcus lysodeikticus cells. Briefly, a 200 unit/mL Lysozyme solution in 50 mM Potassium Phosphate Buffer was added to a 0.015% [w/v] Micrococcus lysodeikticus cell suspension in the same buffer. We then recorded the decrease in A_{450} over 5 minutes. We fabricated nine millipost tips made from 80% lysozyme and 20% PEO 200k and dissolved sets of three millipost tips together. We performed triplicate assays on each dissolved solution for a total of nine tests. We compared the results to the results of a solution made with lysozyme that was not compressed into a millipost tip.

In vivo insulin delivery evaluation

All animal experiments were approved by and performed in accordance with the Committee on Animal Care at MIT. To assess the insulin millipost formulation (including the subcutaneous and gastric administrations without the SOMA device) at Novo Nordisk, we administered the API formulation to Landrace Yorkshire duroc cross-breed pigs (bodyweight 50-100kg) (Novo Nordisk, Denmark). We chose a swine model due to the anatomical similarities of the GI tract to humans as well as its wide use in GI tract, device evaluation. We observed no adverse effects during the experiments. For subcutaneous studies we applied a brief anaesthesia using propofol (1–2 mg/kg BW intravenously) (Rapinovet vet 10 mg/ mL; Schering-Plough Animal Health, Ballerup, Denmark). Insulin milliposts were delivered subcutaneously by creating a guide hole 3 mm deep in the swine's skin using an 18G needle and placing the millipost into the guide hole. For the Intragastric studies we used a combined injection anaesthesia, where the pigs were anaesthetized with 0.06mL/kg BW of (125 mg tiletamine [0.75 mg/kg] and 125 mg zolazepam [0.75 mg/kg], [Zoletil 50; ChemVet, Silkeborg, Denmark] plus 125 mg, xylazine [0.75 mg/kg] [Narcoxyl vet 20 mg/mL; Intervet, Ballerup, Denmark] plus 125 mg ketamine [0.75 mg/kg] [Ketaminol vet 100 mg/mL; Intervet] + 125 mg butorphanol [0.15 mg/kg] [Torbugesic vet 10 mg/ mL; Scanvet, Fredensborg, Denmark]). Animals were supplemented with 1/3 of initial dose every 30 min. The milliposts delivered via an intragastric injection were inserted during a laparotomy procedure in which a 3 cm incision was used to access the gastric mucosa, and a millipost was manually inserted into the gastric surface epithelium. To assess the insulin millipost formulation in the SOMA device at MIT, we administered the API formulation to female Yorkshire swine, 35 kg to 65 kg (Tufts, Medford USA). To deliver the SOMA devices, we placed the swine on a liquid diet 24 hours before the procedure and fasted the swine overnight. We sedated them with intramuscular injection of Telazol (tiletamine/zolazepam) (5 mg/kg), xylazine (2 mg/kg), and atropine (0.05 mg/kg) and if needed supplemental isoflurane (1 to 3% in oxygen) via a face mask. An orogastric tube or overtube was placed with guidance of a gastric endoscope and remained in the esophagus to ease the passage of the device. SOMA devices were passed through the overtube and placed into the insufflated stomach from a height

of 5-7 cm. Although swine were fasted, some swine still possessed food in their stomach during the SOMA delivery. Blood samples collected from SOMA devices which landed on food or did not inject their drug payload after actuation were discarded from the sample (Table S2). Blood samples from all studies at MIT and Novo Nordisk were obtained via a central venous line at designated time points, including but not limited to every 10 minutes for the first two hours and every 30 minutes for hours 2-4. Blood samples were immediately tested for glucose levels using a OneTouch Ultra glucose monitor by LifeScan Inc. (Milpitas, USA). Additional blood was collected into Ethylenediaminetetraacetic K3 tubes (Sarstedt, Numbrecht, Germany) and spun down at 2000 Relative Centrifugal Force for 15 minutes. Collected plasma from MIT was shipped on dry ice to Novo Nordisk in Maalov, Denmark, and all blood was analyzed there via an AlphaLisa developed at Novo Nordisk. Briefly, the homogenous bead assay employed two monoclonal antibodies against human insulin, creating an acceptor-bead, insulin, and donor-bead layering. This generated a signal which was proportional to the concentration of insulin. This test is specific for human insulin and does not detect other endogenous insulins (Fig. S15).
The amount of insulin inserted into the tissue via the SOMA device was estimated using histology results from in situ experiments (Fig. 3f). Because the SOMA milliposts shafts and tips were made from 100% human insulin, not all of the API was considered as payload. The millipost insertion depth was evaluated and used to calculate the volume of the millipost which was submerged in the tissue. This volume was then multiplied by the density of the millipost to estimate the amount of API delivered. The amount of human insulin delivered by the manually placed milliposts, made from 80% human insulin and 20% PEO 200k, were assumed to be 100% of the incorporated API because the entire milliposts were inserted into the tissue.

In vivo retention and safety evaluation

Six SOMAs with 32G stainless steel needles permanently fixed protruding 3 mm out of the bottom of the device were placed in the stomach of a swine using an overtube. While these devices were still inside of the stomach, we simulated translational swine movements (to mimic the outside forces as described in the "Simulated Walking Test" methods section) the device might experience while inside of the body. An endoscopy was then performed to check for any bleeding caused by the needles. Daily radiographs were subsequently performed to determine residency time of the devices as well as for any evidence of gastrointestinal perforation (pneumoperitoneum). X-rays were taken until all devices passed. Additionally, during retention of the devices the animals were evaluated clinically for normal feeding and stooling patterns. Reassuringly, there was no evidence of pneumoperitoneum on x-ray nor any changes in feeding or stooling patterns.

Rat toxicity test

Acute Toxicity Study: Three rats (Charles River Labs, Sprague Dawley 400-450 g in weight) were dosed once with 2000 mg/kg of stainless steel particles (McMaster Carr Elmhurst, USA) measuring between 100 and 300 μm in diameter, in 1 mL of soybean soil (Crisco Orrville, USA). These rats were compared to a control group of three rats which were only dosed with 1 mL of soybean oil. After 14 days, both groups were euthanized via an overdose of inhaled carbon dioxide and a necropsy was performed and samples of heart, lung, stomach, small intestine, colon, liver, kidney, spleen, pancreas and bladder were fixed in formalin, stained using H&E and analyzed by a pathologist to determine if any abnormalities were noted.

Sub chronic Study: Six rats (Charles River Labs, Sprague Dawley 330-450 g in weight) were dosed, via oral gavage, with 80 mg/kg of stainless steel particles, measuring between 100 and 300 μm in diameter, in 1 mL of soybean oil five days per week for four weeks. These rats were compared to a control group of six rats which were only dosed with 1 mL of soybean oil for the same frequency and duration. Whole blood samples were taken at days 1, 15, and 26 and tested for traces of chromium and nickel. Urine samples were taken at day 15 to test for traces of chromium and nickel as well. Radiographs of the GI tract were taken using a Faxitron Multifocus (Faxitron, Tucson, USA) at day 8 to confirm passage of the stainless steel. At the end of the study, on day 26, all 12 rats were euthanized via an overdose of inhaled carbon dioxide and a necropsy was performed. Samples of heart, lung, stomach, small intestine, colon, liver, kidney, spleen, pancreas and bladder were fixed in formalin, stained using H&E and analyzed by a pathologist to determine if any abnormalities were noted.

Histology:
Tissue samples were placed in a bath of 10% neutral buffered formalin (VWR) for 72 hours and then placed into a bath of 70% ethanol (VWR). After fixing the tissue, we embedded the sample in paraffin and cut 4 μm slices of the tissue using a microtome (Leica Biosystems, Wetzlar, Germany). We then placed the samples on glass slides and stained the tissue as described in the text.

Supplementary Text

Computational optimization:
We created the optimized shape by performing a two dimensional curve optimization over a 180 degree plane in quadrants I and IV and revolving the curve, described by a planar curve C in polar coordinates (r,θ), about the Y axis. Fig. S16 illustrates the optimized curve as well as the vectors and methods described in this section. As an initial guess for the shape, we utilized mathematical models for tortoise shells, which combined a superellipse or hyperbola to represent the upper portion and a low curvature arc to represent the bottom. MATLAB's fmincon function along with a custom MATLAB code was used to perform the optimization. The optimization protocol optimized for the lowest mean orientation time of a shape when released from a series of random orientations. This was calculated by finding the minimized area under the curve presented in Fig 2b. The protocol at the same time maximized the amount of torque required to push the device from its preferred orientation. Because these two competing functions were being optimized at the same time, the resulting device may not orient the quickest of all possible shapes; however, it would be the most optimized to both orient and resist external forces. This presents the most optimized shape for the application at hand.
The fmincon optimization function varied the radius of 25 different points spaced apart at equal angles along a curve drawn in polar coordinates.
When reconverted into Cartesian coordinates, the space inside the revolved curve and below the X-Z plane was set to contain high density material (7.7 g/cm^3) while space above the X-Z plane and inside the revolved curve was set to contain low density material (1.1 g/cm^3). To simulate a hollow top section, a 4 mm in radius cylinder centered about the Y axis, beginning at the X-Z plane and ending at the curve boundary was removed from the top portion of the shape. The mass of the spring and the millipost were incorporated into the model. In order to define a scale for the shape we constrained the center of mass to the origin and the highest possible point to the coordinate [0,1]. We then scaled the final shape to fit the size constraints. These constraints

matched the requirements of an axisymmetric mono-monostatic shape, so no possible solutions were lost.
The optimization itself utilized Newton's kinematic equations to find a given shape's self-orientation time, t:

$$\Delta\theta = \omega t + \frac{1}{2}\alpha t^2 \quad \text{Equation (1)}$$
$$\alpha = \tau / I \quad \text{Equation (2)}$$
$$\omega = \omega_0 + \alpha t \quad \text{Equation (3)}$$
$$I = \int r^2 dM \quad \text{Equation (4)}$$
$$\tau = d * F * \sin(\theta) \quad \text{Equation (5)}$$

where angular acceleration α, and angular velocity ω, are determined based on the device's moment of inertia I, and torque τ. The gravitational force F, acted as the external force in the model and was used to calculate the simulated torque applied to the lever arm d, defined as the distance between the device's center of mass and point of contact with the tissue wall.
The angular acceleration of the device at a given orientation, defined by equation 2, determines the orientation speed and varies with torque and moment of inertia. We calculated the moment of inertia along with the total weight of the device by breaking the 3D space up sinto a 50x50x50 array of equally sized blocks, assigning a density to each block, and performing a summation described in equation 4.
Calculating the torque on the device required determining both the direction and magnitude of the force and distance vectors as per equation 5. We defined the force vector as the gravitational force on the object starting from the center of mass and pointing in a direction perpendicular to the surface of contact. We calculated the distance vector as the distance between the center of mass and the pivot point of the device on the surface of contact. When determining the pivot point, we took into account the greater curvature of the device, as areas with concave curvature do not touch the surface.

Sucrose barrier dissolution modeling

We calculated the radius at which the sucrose barrier would propagate a crack using Griffith's criterion: $\sigma_c^2 = \frac{2\gamma E}{\pi a}$, where σ_c is the critical stress applied by the spring, γ is the surface energy of the material, E is the Young's modulus of the material, and a is the surface area perpendicular to the applied stress. Because all variables in the equation remain constant aside from the surface area, the dissolution rate defines the time until the cracking event and spring release. The COMSOL models and experimental testing are based on a spring that provides 1N of force. The physical spring was created by cutting a purchased spring into the appropriate size.
COMSOL Multiphysics (Stockholm, Sweden) was used to mathematically model the dissolution of a sucrose cylinder in both still water and water that flowed at 0.02 m/s, similar to that of the human stomach (44). Fick's law was used to estimate the rate of the diffusion process at the shrinking boundary between the sucrose and the water. Diffusion coefficient of $5.2*10^{\wedge -10}$ m^2/s, an equilibrium concentration for sucrose in water of 6720 mol/m^3, and mass transfer coefficient of $7.8*10^{-4}$ m/s (found experimentally) were used as parameters. The COMSOL model was run at starting sucrose cylinder diameters of 6 mm, 5 mm, and 4 mm, and the time it took for the cylinder to dissolve to a diameter of 1.7 mm was used to predict the actuation timing if a spring had been present in the cylinder.

To calculate the mass transfer coefficient of sucrose in water, sucrose was caramelized at 215°C for 15 minutes in a PDMS mold with a 6 mm in diameter hole to create a cylindrical shape. The caramelized sucrose cylinder was placed in a 500 mL beaker of water at room temperature, and the diameter of the sucrose was measured every minute. The rate of dissolution was modeled and the slope of the linear fit was determined to be the mass transfer coefficient.
In order to test the dissolution of the sucrose barrier on springs, sucrose encapsulated springs were placed in 500 mL beaker of water at room temperature, and the timing of the spring actuation was recorded for 4 mm, 5 mm, and 6 mm diameter sucrose spring, with three trials each.

SOMA Membrane

To aid in protecting the SOMA from gastric content, a valved silicone membrane was placed inside the bottom section of the device (Fig. S12). When food and water was placed on top of the membrane in vitro, the valve prevented them from passing through. The millipost, however, passed through the valve with 0.03 ± 0.02 N of force. When tested in vitro, the new piece did not affect the actuation of the device, and it prevented food or liquid from entering the inner chamber of the SOMA.

Additionally, due to the device's high density, it possessed the ability to pass through food particles suspended in a liquid and localize to the stomach wall. We recorded that 20 SOMA devices dropped into a food particle bath 20 cm in height containing 3 mm in diameter or smaller particles all reached the bottom of the mixture and self-oriented. We performed this experiment by combining 4 ounces roast beef, a 2 ounce dinner roll, and 2 ounces of cooked spinach prepared by Aramark at the Koch Café with 8 fluid ounces of water. The materials were blended for 30 seconds on high and poured into a 4 cm in diameter container up to a height of 20 cm. SOMA devices were then dropped into the mixture and imaged after they reached the bottom to determine their orientation.

SOMA excretion:

We evaluated integrity of the SOMA device as function of passage through the swine GI tract by dosing 3 SOMA devices without drug per animal to 3 separate swine. All SOMA devices were radiographically confirmed as being excreted. Eight of the 9 administered SOMAs were identified in the feces without any visible damage to the components. The ninth SOMA was inadvertently disposed during cage cleaning. Of note, the SOMA as a whole as well as each piece is smaller than the non-degradable OROS capsule, a device with an obstruction rate of 1 in 29 million that is approved by the FDA for daily delivery. SOMAs persisted in the stomach for up to 9 days in swine (Fig. S11), but device retention could be attributed to slow gastric emptying times in swine *(37)*. Swine possess gastric emptying times on the order of 24 hours or longer while humans and dogs possess emptying times on the order of 0-4 hours. Further tests will be required in other pre-clinical models such as dog and human subjects to assess relevant excretion timelines.

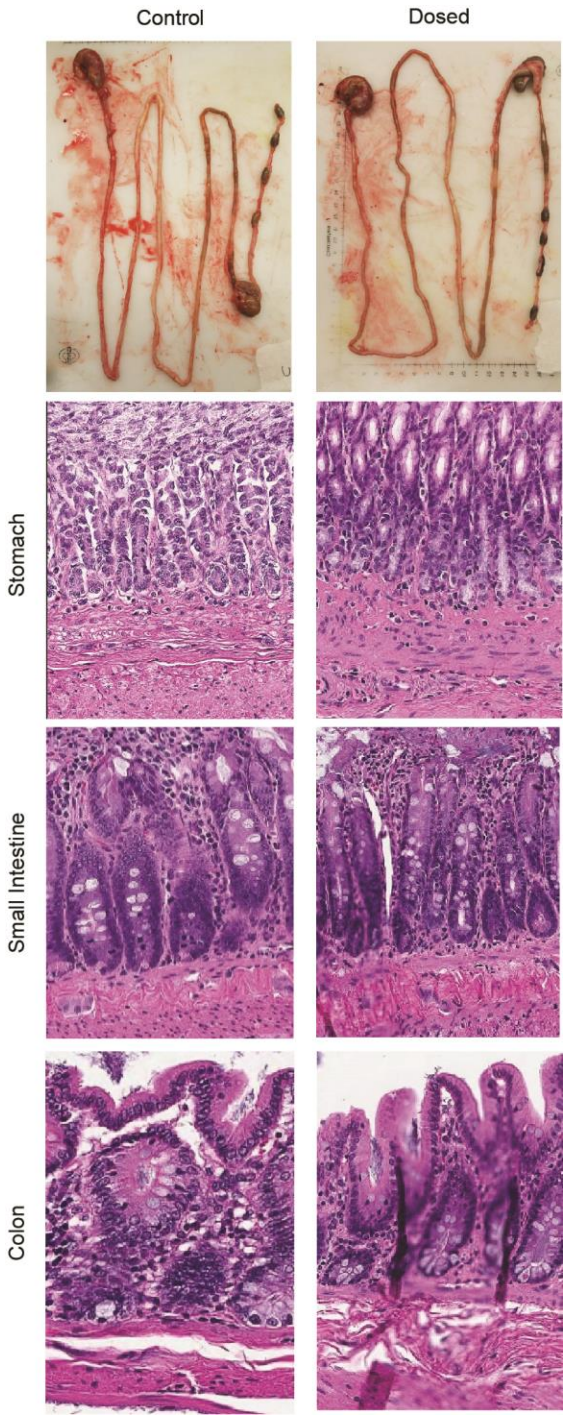

Fig. S1: Stainless steel toxicity examination. Histology from the digestive tract of one of six rats fed a single dose of 2000 mg/kg 316 stainless steel particles suspended in 1 mL canola oil via a 15G oral gavage shows no abnormalities when compared to a rat dosed only with 1 mL of canola oil.

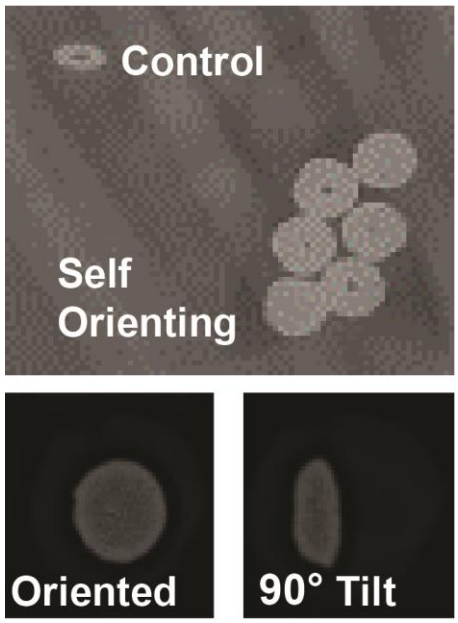

Fig. S2: X-ray of SOMA shape in vivo. Six SOMA devices were fed to a pig along with one control device with the same SOMA shape but a homogeneous density. Due to the circular metal bottom of the SOMA, the devices showed up on an X-ray as a full circle when fully oriented and as a waning circle when not oriented. The control device was also marked with a thin metal washer. The pig was then rotated axially up to 180° as well as tilted in other directions up to 30° to simulated ambulation and extensive motion stress. The pig was then X-rayed. This process was repeated 10 times, and yielded a 100% correction orientation rate for SOMA devices and a 50% orientation rate for control devices.

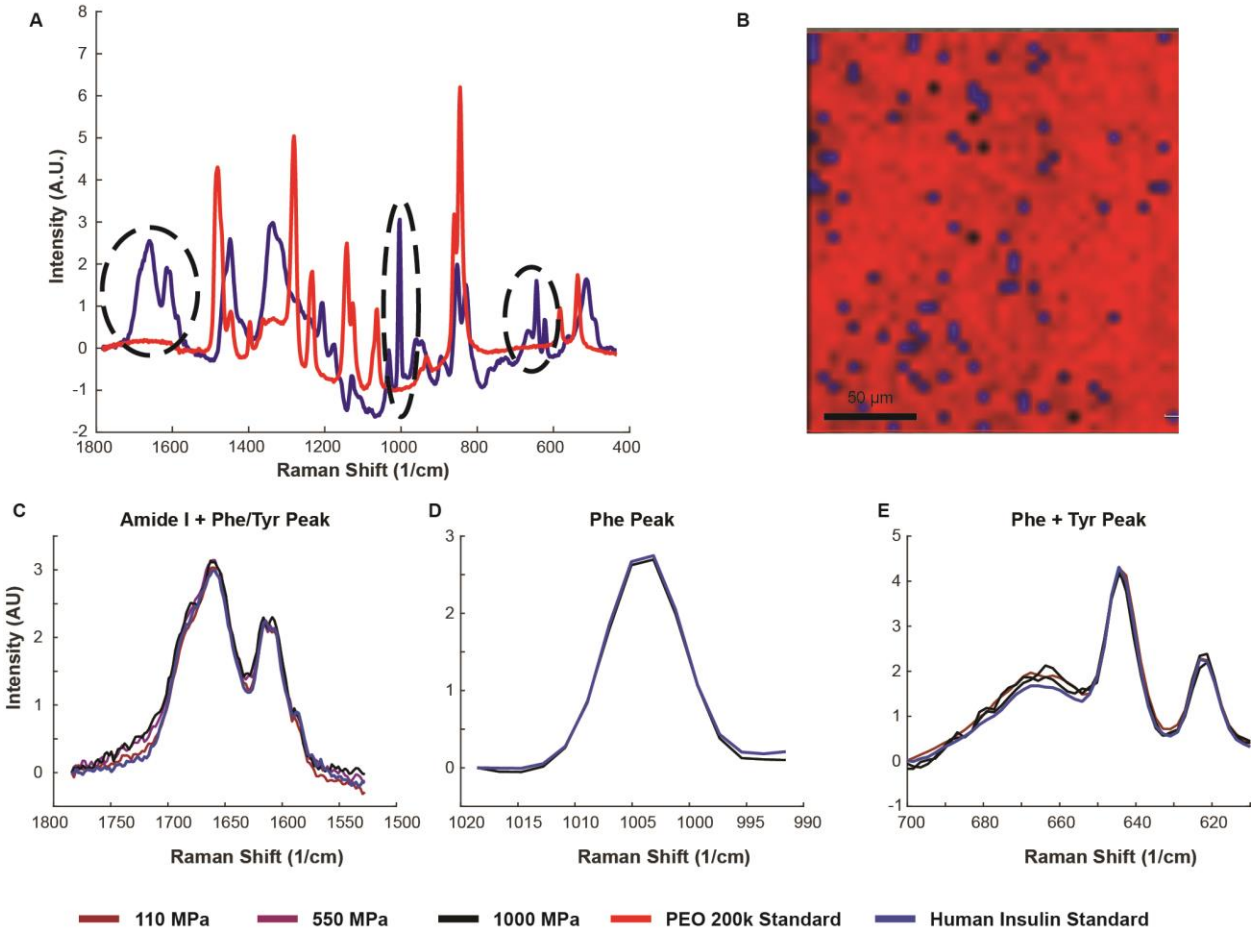

Fig. S3: Raman spectroscopy analysis of compressed insulin. Several milliposts were fabricated of compressed insulin and PEO at varying pressures. These API mixtures were analyzed using Raman spectroscopy to determine if any protein folding changes occurred during exposure to high pressures. (A) Standards of human insulin and PEO 200k. Black circles represent peaks present in the insulin reading that are not present in the PEO reading. These peaks are analyzed in figures (C-E). (B) The differences between the two components allowed for an imaging software to generate a visualization of the mixture using built in pre-processing and chemometrics. In this picture, the blue areas contain greater amounts of PEO. The insulin Raman bands overlapped with the PEO bands over all but five bands: (C) The Amide I band occurring at 1660 cm-1; a Tyr peak occurring at 1613 cm-1; (D) a Phe peak occurring at 1003 cm-1 ; (E) the Phe peak occurring at 622.5 cm-1; and the Tyr peak occurring at 644.3 cm-1. No band shifts or width increases were observed demonstrating that there were no protein folding changes.

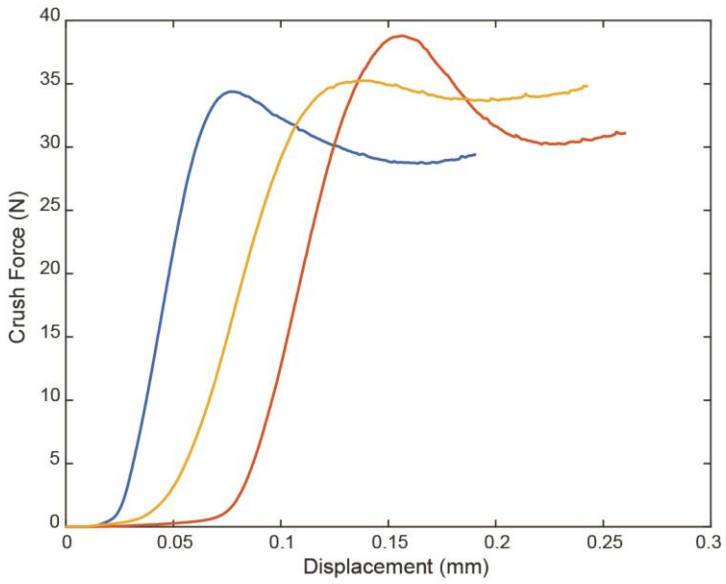

Fig. S4: Compressed insulin needle crush test. Cuboid shaped pellets with the dimension of 3.3 x 0.55 x 0.55 mm3 were fabricated from the described insulin/PEO 200k mixture. These pellets, while undergoing a crush test, demonstrated a Young's modulus of 730 ± 30 MPa. This is similar to the Young's modulus of PEO. The ultimate strength of the pellet is 36 ± 2 N.

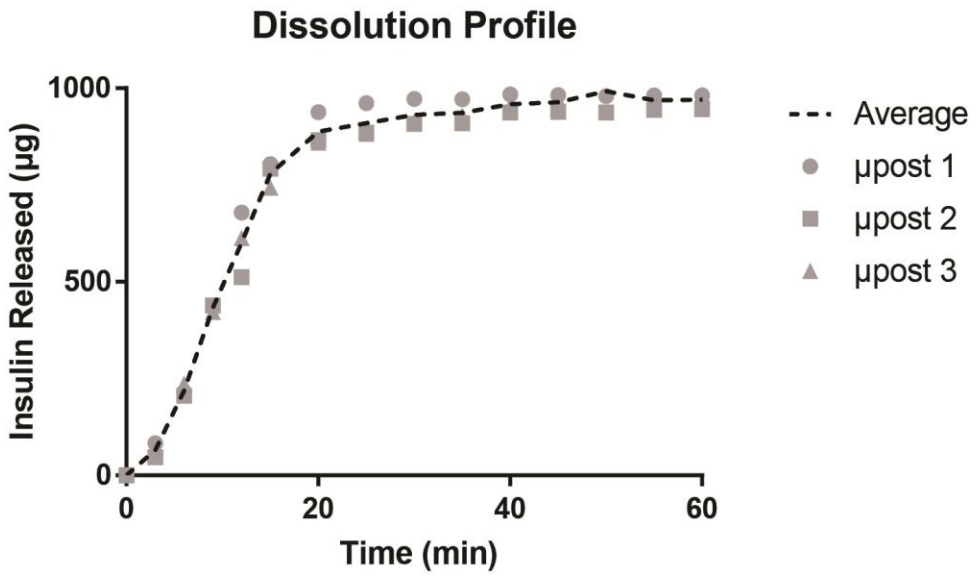

Fig. S5: Millipost dissolution profile. milliposts containing 80% Human Insulin and 20% PEO 200k by weight were dissolved in a falcon tube containing 2 mL of PBS at 37ºC shaken on a lab shaker at 50 rpm. 200 µL was sampled every three minutes for the first 15 minutes and every 5 minutes thereafter, and the removed liquid was replaced with fresh PBS. Complete dissolution occurred within 1 h.

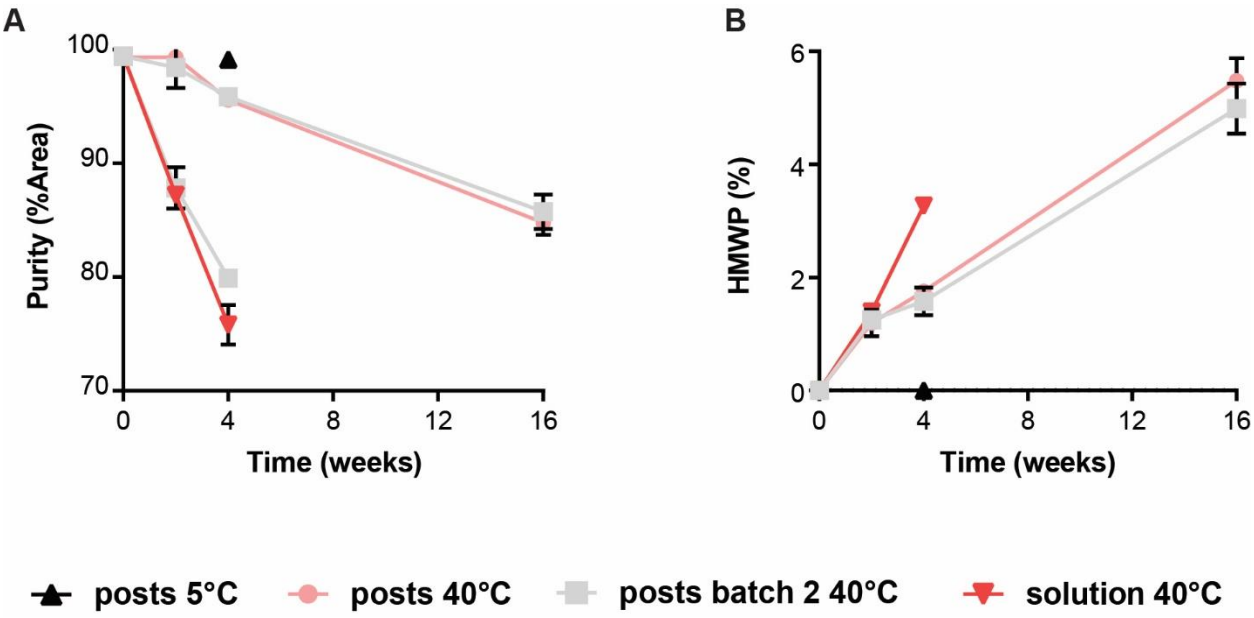

Fig. S6: millipost API stability studies. (A) Insulin purity and (B) high molecular weight protein (HMWP) concentration during 16 weeks of stability testing (n=3, Error Bars = SD).

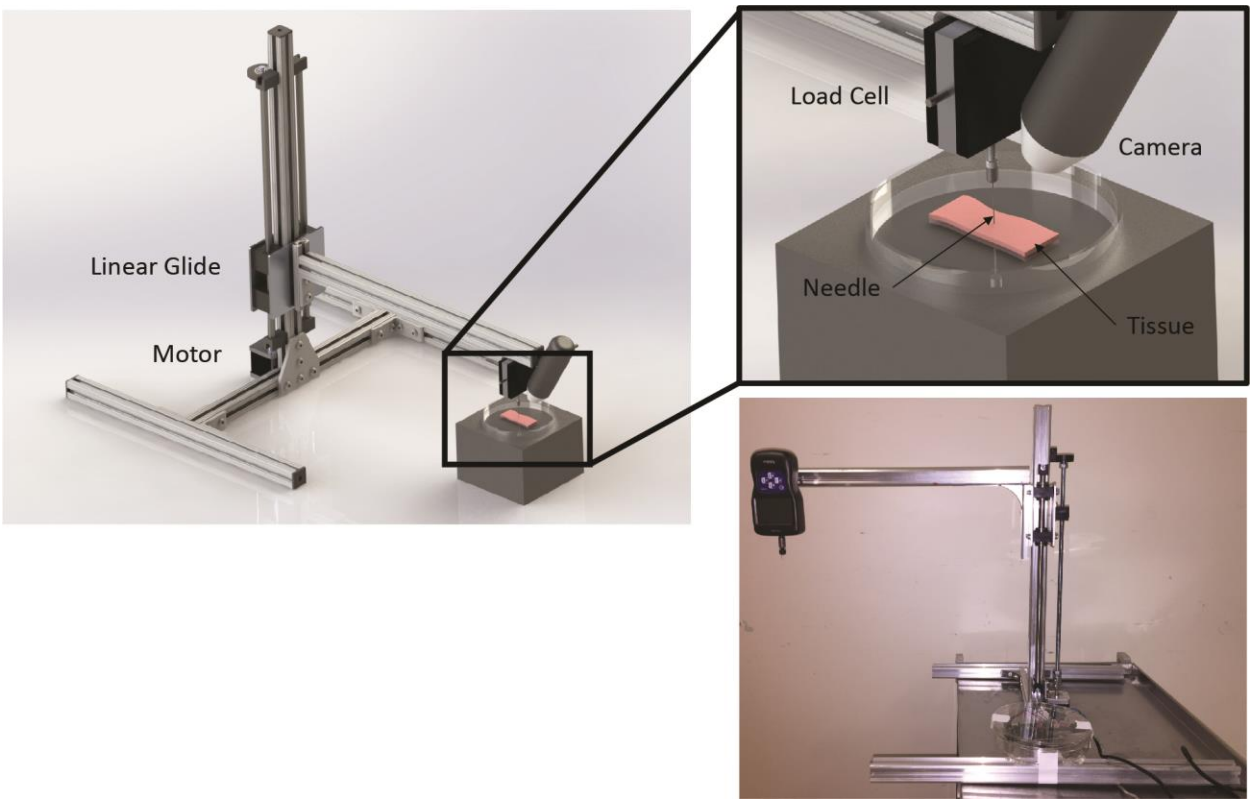

Fig. S7: Schematic and photograph of needle insertion mechanism. In vivo insertion data and ex vivo insertion data requiring video was acquired using the following device consisting of a linear glide, stepper motor, 0.5 N or 10 N load cell and video camera. The lower right picture shows the 10 N load cell attached to the device. All of the devices were controlled via a custom-made LabView setup.

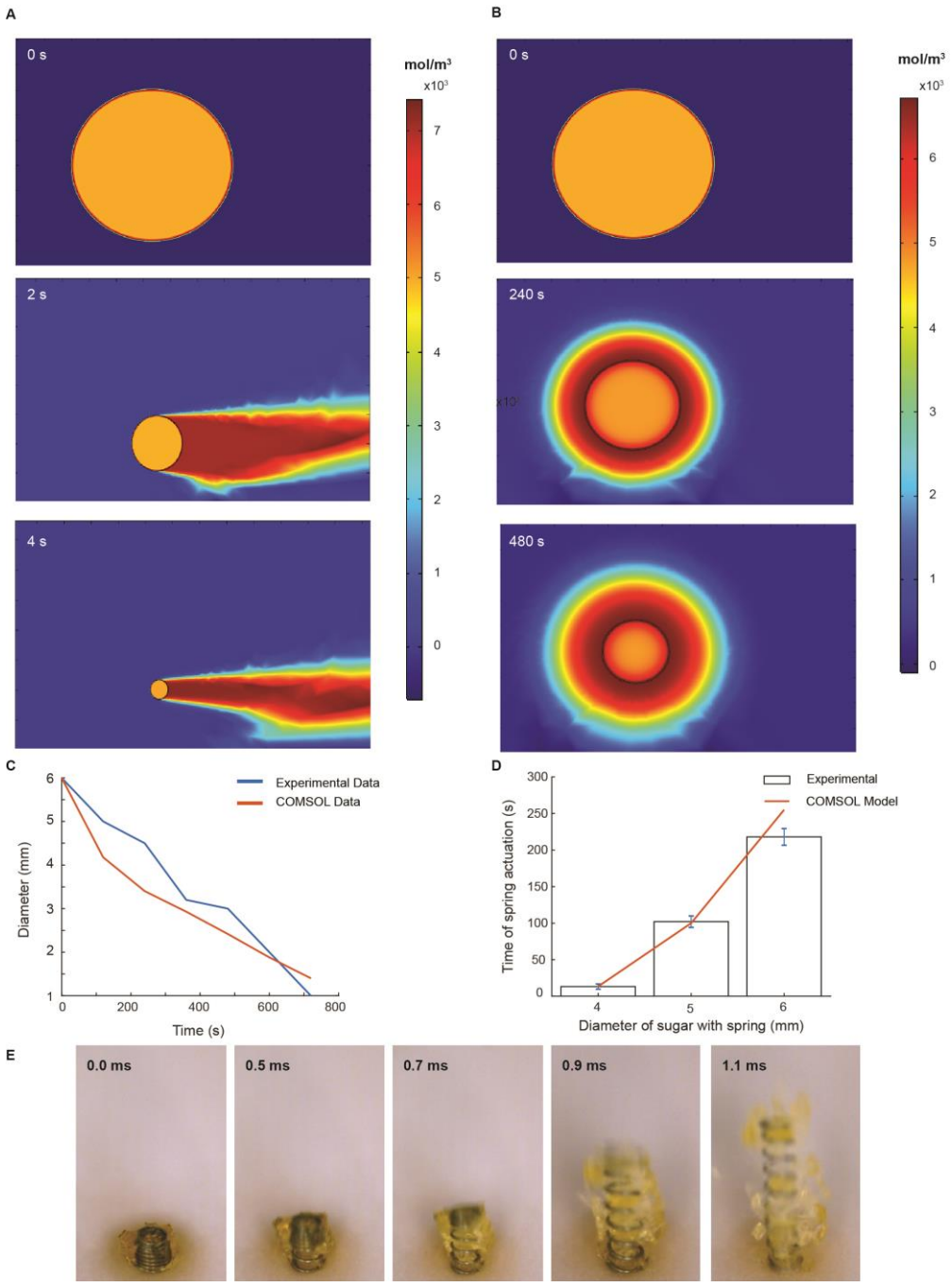

Fig. S8: Characterization of sucrose actuation mechanism. Concentration gradient of sucrose modeled in COMSOL Multiphysics as sucrose cylinder dissolves in an infinite body of (A) water flowing at a velocity of 0.02 m/s and (B) water without convection. The black circle indicates the shrinking boundary of the sucrose cylinder, and concentration is shown in units of mol/m3. (C) Rate of dissolution of sucrose cylinder over 4 trials; slope indicates mass transfer coefficient between water and sucrose. (D) The time measured from when a sucrose coated spring is submerged in DI water until it actuates. The bars represent the experimental actuation time (n=3, Error bars = SD) and the line represents the time predicted by COMSOL. (E) High speed image of spring popping out of sucrose coating as DI water is dripped on it from above.

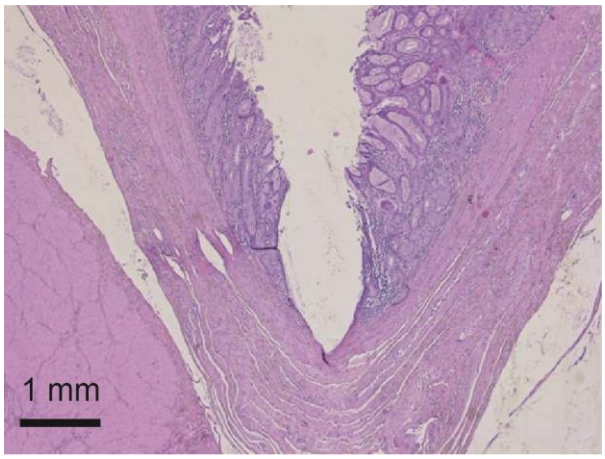

Fig. S9: In vivo SOMA histology. Histology from a biopsy taken after an in vivo SOMA insertion event.

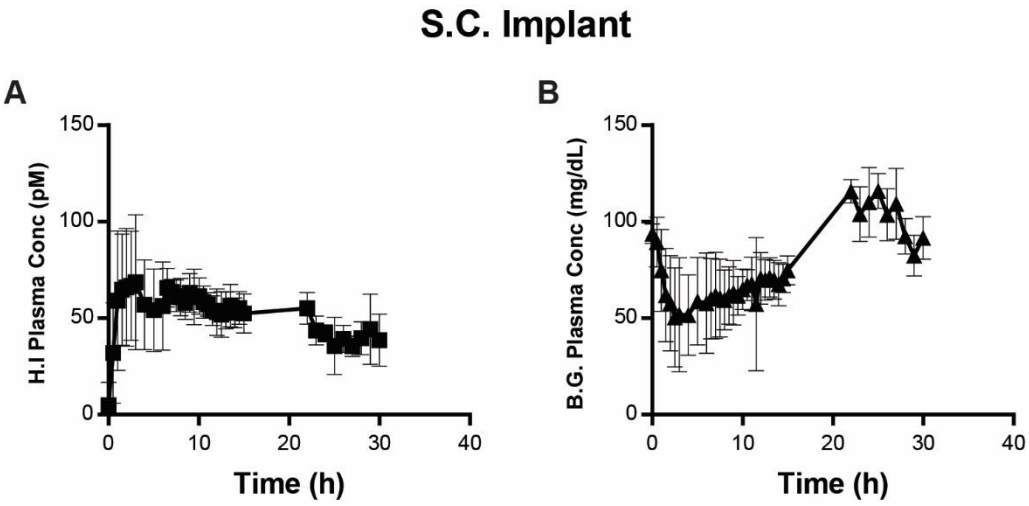

Fig. S10: In vivo millipost delivery. (A) millipost shafts inserted into the subcutaneous (S.C.) space deliver insulin for 30 hours (n=6, Error Bars = SD). (B) Sustained BG lowering is seen throughout the first 15 h. The swine were fed at hour 22, causing a B.G. spike. These implants do not have a sharp tip and are instead a 1.2 mm in diameter rod that is 1 mm in height.

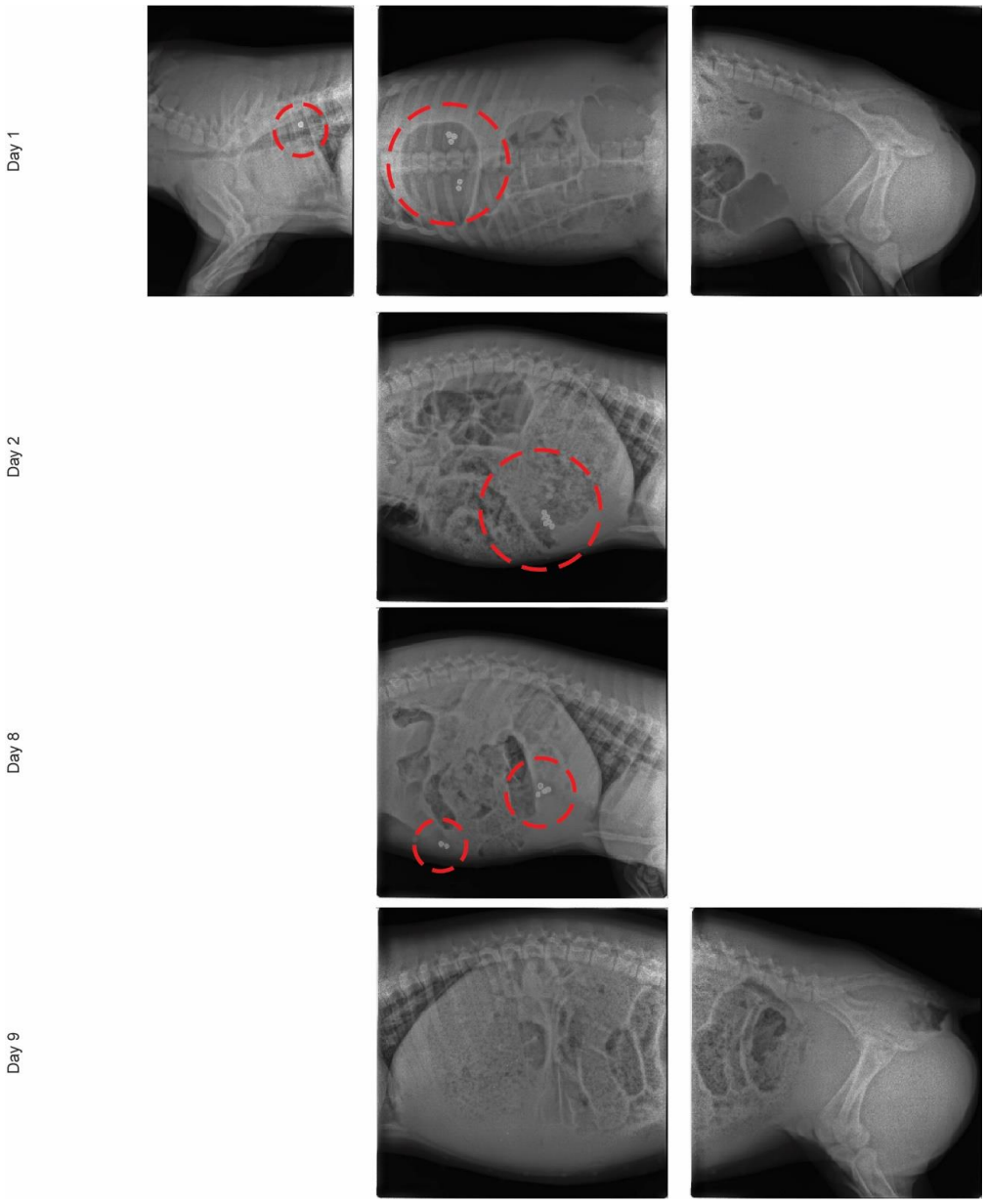

Fig. S11: Gastro-retentive properties of SOMA devices. Six SOMA devices are shown to pass through a swine's GI tract in 8 days. The SOMA devices spend days 1-7 in the stomach. The day 1 x-ray shows one SOMA device being delivered through the esophagus and 5 soma devices in the stomach. On day 2, all of the SOMA devices are in the stomach, and they remain there until day 7. On day 8, 4 SOMA devices are shown to have moved into the intestines. By day 9, there are no SOMA devices present in the x-rays. This indicates that the SOMAs have passed out of the swine. The pig showed no signs of obstruction throughout the experiment. Integrity of the SOMA device following GI transit was confirmed by examination of SOMAs recovered after excretion in a separate study. The SOMAs persisted in the stomach for up to 9 days in swine, but device retention could be attributed to slow gastric emptying times in swine. Further tests will be required in other pre-clinical models such as dog and eventually human subjects to assess relevant transit timelines. See supplementary text for additional information.

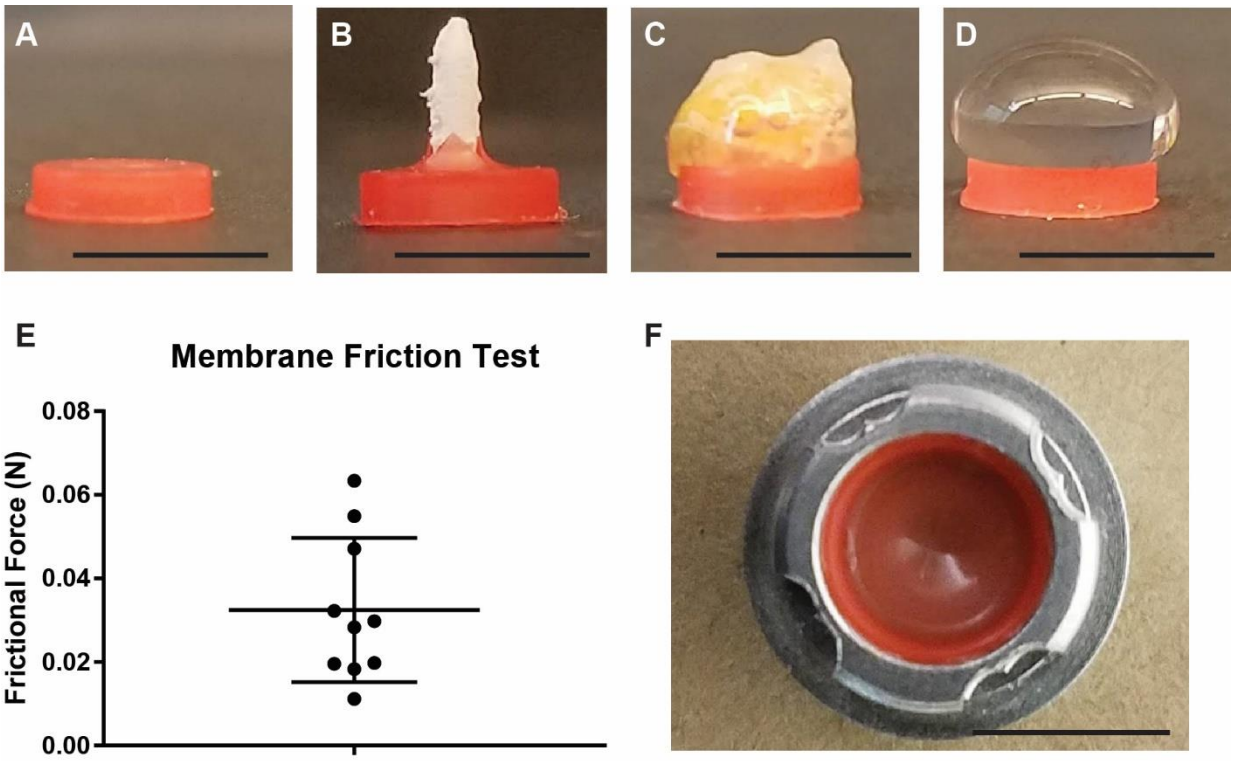

Fig. S12: Membrane coating on SOMA prevents food and liquid from entering the millipost chamber. (A) SOMA membrane is made by casting Elastosil M 4642 B in an aluminum mold and cutting perpendicular slits for the millipost to pass through. (B) Millipost passes through the slits in the membrane. (C) Chewed pear is prevented from passing through the membrane. (D) Water is prevented from passing through the membrane. (E) Force experienced bythe millipost when passing through the membrane is 2 orders of magnitude less than the force applied by the actuation spring (n=10, Error Bar = SD). (F) The membrane fits snuggly into a cavity in the SOMA bottom piece. Scale bars are 5 mm. See Supplementary text for additional information.

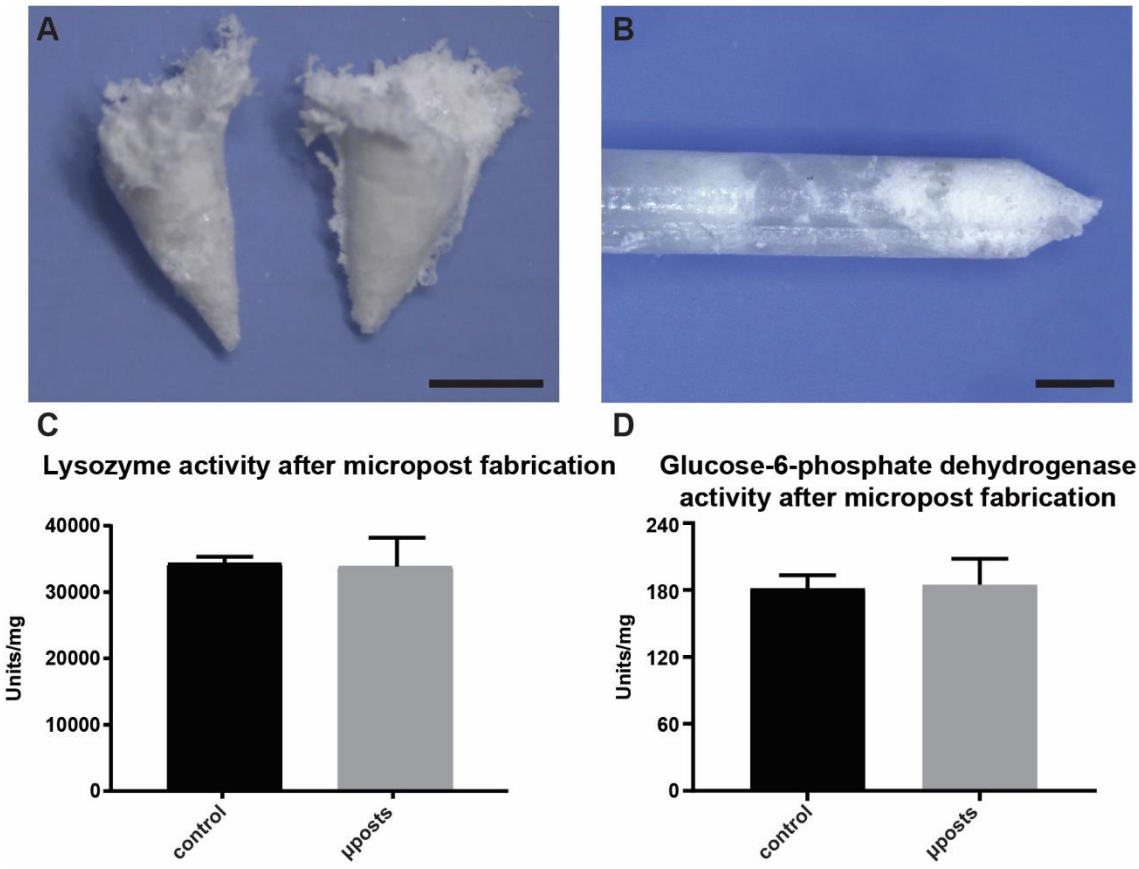

Fig. S13: Enzymatic activity assays of fabricated milliposts. millipost tips created with (A) 80% lysosyme and 20% PEO 200k (n=9 milliposts divided into three groups dissolved in three separate solutions) and (B) 40% glucose-6-phosphate-dehydrogenase and 60% PEO 200k were dissolved (n=3 milliposts dissolved into one solution which was evaluated), and (C-D) enzymatic activity assays were performed to ensure that the proteins remained active after the manufacturing process. The control represents uncompressed powder. Scale bar is 1 mm. (Error bar = SD).

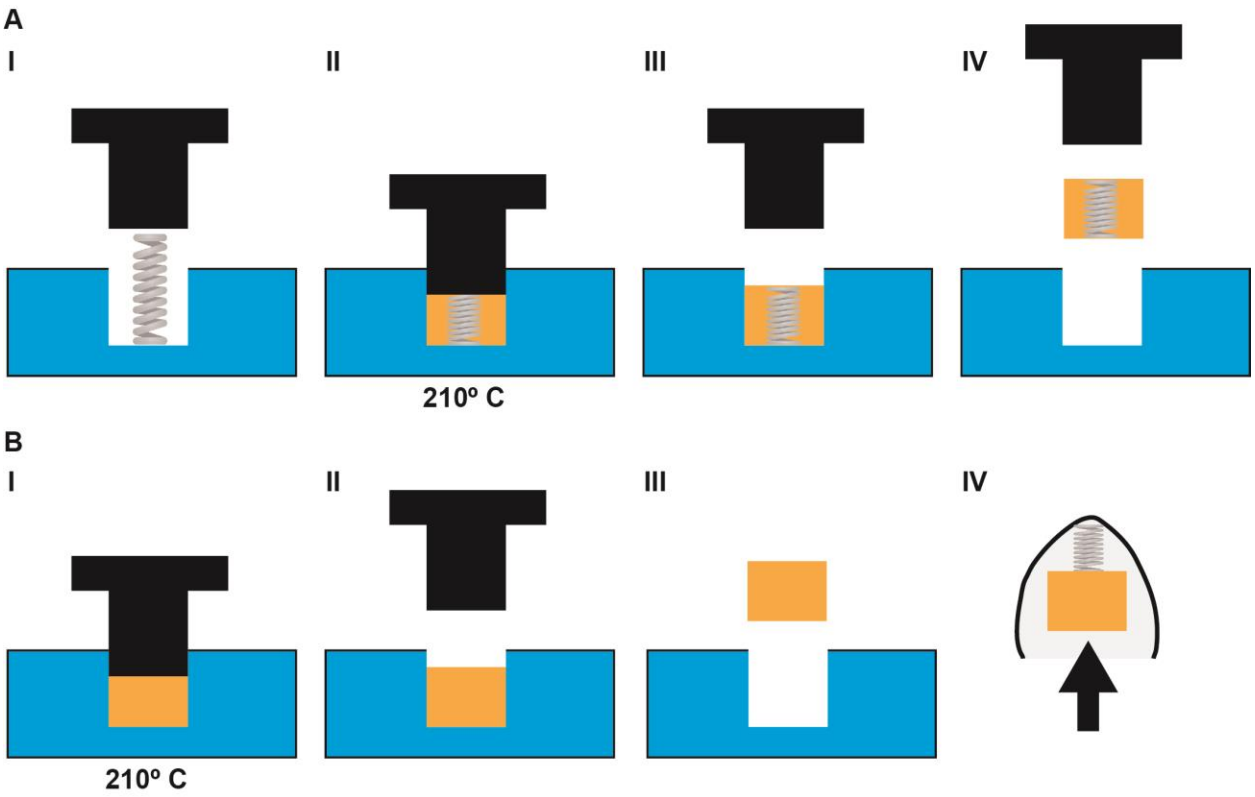

Fig. S14: Sugar actuator work flow. (A) Sugar encapsulated springs were fabricated in a short four step process. (I) A compression spring was placed in a silicone mold and (II) caramelized sucrose heated to 210º C for 15 minutes in an oven was poured into the mold. Isomalt was also used. A custom-made plunger compressed the spring into the caramelized sucrose and the mold was left to cool for several minutes. (III) The plunger was then removed and (IV) the sucrose encapsulated spring was pulled out of the mold. The size of the hole in the mold determined the width of the sugar encapsulated spring. (B) Springs compressed with sugar were fabricated via a similar process.

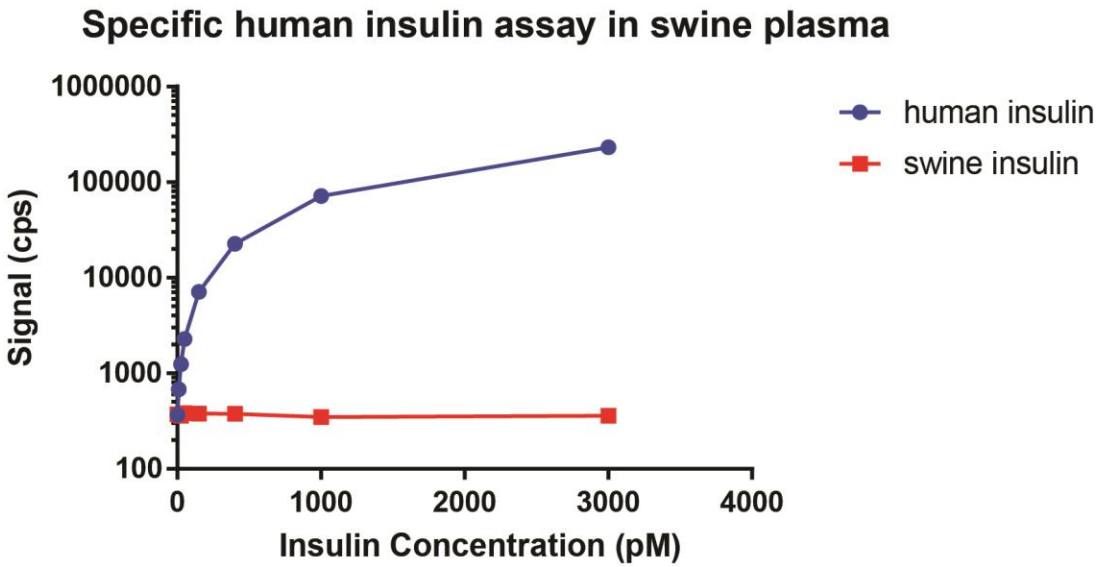

Fig. S15: Insulin quantification assay. The ELISA and AlphaLisa experiments utilize a homogeneous bead assay that employs two monoclonal antibodies against human insulin. The assay is specific to human insulin over swine insulin.

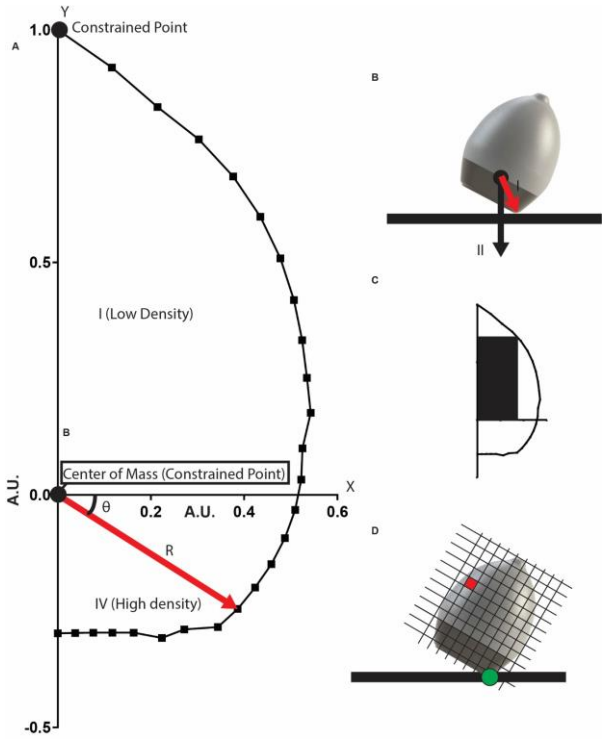

Fig. S16: Computational results from self-orientating shape optimization. a) This curve is the result of the optimization analysis performed as described in the methods section of this paper. Each point represents a polar coordinate where the angle was fixed and the radius was varied by MATLAB's fmincon function. The red line labeled "R" represents the radius vector, and the angle θ is also labeled. The curve is scaled to its appropriate size and revolved about the Y axis to make the 3 dimensional shape used for the SOMA device. Areas with negative Y values located in quadrant IV represent portions of the device made with stainless steel, while areas with positive Y values located in quadrant I represent portions of the device made with hollowed out PCL. Small modification were made to create the final device. These modifications include curve smoothing to ease manufacturability as well as cutting slits to allow for water to reach the sugar encapsulated spring. Additionally, the top portion of the device was flattened slightly to add room for the compressed spring inside of the device. b) This figure defines the two vectors described in the optimization methods section. The center of mass is the black circle. Vector (I) in red is the distance vector which emanates from the center of mass. Vector (II) in black is the gravitational force vector which emanates from the center of mass. The cross product of vectors (I) and (II) yields the torque. c) This figure represents an example of the process used to hollow out the inner portion of the shape in the simulation. The black rectangle would be set to contain no mass. d) This figure demonstrates the method of calculating the moment of inertia. This figure is only in two dimensions, but the shape is cut in the third dimension as well. Each cube is defined as being part of the high density section, the low density section or as not part of the shape. First the mass of a cube (an example cube is marked in red on the figure) is calculated using its size and defined density. Next, the distance between the center of the cube and the point of rotation of the shape, marked as a green circle, is calculated. The moment of inertia of the cube as a part of the rotating shape is then calculated by squaring the distance and multiplying that value by the mass of the cube. The moment of inertia of each cube is summed to get the total moment of inertia.

Sample	Amide I Pos/Width	Tyr Pos/Width	Phe Pos/Width	Tyr Pos/Width	Phe Pos/Width
Standard	1660/56.1	1613/18.5	1003.4/7.7	644.3/10.0	622.5/7.7
110 MPa	1660.6/54.8	1614.3/16.5	1004.9/7.5	644.3/10.0	623.1/8.1
550 MPa	1658.7/59.0	1616.3/17.4	1003.0/7.0	644.3/10.1	621.2/6.8
1000 MPa	1658.7/57.1	1618.2/18.2	1004.9/7.8	644.3/8.7	621.2/7.4

Table S1: Raman spectroscopy analysis. Peak heights and widths measurements denoted in Fig. S2.

SOMA device #	Endoscopic Observations
1	Stomach covered in 5 mm layer of solid swine food. SOMA dropped from 2 cm above tissue. Lands on tissue wall. Remains upright. Actuates but μpost does not insert into wall. No insulin in blood samples and B.G. drop not realized. (Point removed from data set for SOMA delivery in Fig 4).
2	Large amount of fluid in stomach. SOMA dropped from 2 cm above tissue. Lands on tissue wall and is submerged in large puddle of fluid. Remains upright. Visualization of actuation but not injection. Insulin not shown in blood samples and B.G. drop realized. (Point removed from data set for SOMA delivery in Fig 4).
3	Clean stomach. SOMA dropped from 2 cm above tissue. Lands on tissue wall. Remains upright. Visualization of actuation and injection. Insulin shown in blood samples and B.G. drop realized.
4	Clean stomach. SOMA dropped from 2 cm above tissue. Lands on tissue wall and slides into a stomach fold. Remains upright. Insulin shown in blood samples and B.G. drop realized.
5	Clean stomach. SOMA dropped from 2 cm above tissue. Lands on tissue wall. Remains upright. Visualization of actuation and injection. Insulin shown in blood samples and B.G. drop realized.

Table S2: Endoscopic observations from SOMA delivery.

Specification	Spring 1	Spring 2	Spring 3
Diameter (mm)	2.2	2.2	2.3
Free Length (mm)	13.3	10.9	10.5
Compressed Length (mm)	1.6	1.75	2.55
K (N/mm)	0.19	0.55	1.1
Coils	8	7	7
Wire Diameter	0.2	0.25	0.3
Compressed Force (N)	2.2	5	9

Table S3: Custom spring specifications

Movie S1: Video of SOMA prototype self-orienting.

References and Notes

1. L. Fallowfield, L. Atkins, S. Catt, A. Cox, C. Coxon, C. Langridge, R. Morris, M. Price, Patients' preference for administration of endocrine treatments by injection or tablets: Results from a study of women with breast cancer. *Ann. Oncol.* **17**, 205–210 (2006). doi:10.1093/annonc/mdj044 Medline

2. G. A. Harrison, Insulin in Alcoholic Solution by The Mouth. *BMJ* **2**, 1204–1205 (1923). doi:10.1136/bmj.2.3286.1204 Medline

3. Diabetes Control and Complications Trial Research Group, The effect of intensive treatment of diabetes on the development and progression of long-term complications in insulin-dependent diabetes mellitus. *N. Engl. J. Med.* **329**, 977–986 (1993). doi:10.1056/NEJM199309303291401 Medline

4. M. J. Calvert, R. J. McManus, N. Freemantle, Management of type 2 diabetes with multiple oral hypoglycaemic agents or insulin in primary care: Retrospective cohort study. *Br. J. Gen. Pract.* **57**, 455–460 (2007). Medline

5. E. Caffarel-Salvador, A. Abramson, R. Langer, G. Traverso, Oral delivery of biologics using drug-device combinations. *Curr. Opin. Pharmacol.* **36**, 8–13 (2017). doi:10.1016/j.coph.2017.07.003 Medline

6. E. Moroz, S. Matoori, J.-C. Leroux, Oral delivery of macromolecular drugs: Where we are after almost 100years of attempts. *Adv. Drug Deliv. Rev.* **101**, 108–121 (2016). doi:10.1016/j.addr.2016.01.010 Medline

7. T. A. S. Aguirre, D. Teijeiro-Osorio, M. Rosa, I. S. Coulter, M. J. Alonso, D. J. Brayden, Current status of selected oral peptide technologies in advanced preclinical development and in clinical trials. *Adv. Drug Deliv. Rev.* **106**, 223–241 (2016). doi:10.1016/j.addr.2016.02.004 Medline

8. D. J. Brayden, M.-J. Alonso, Oral delivery of peptides: Opportunities and issues for translation. *Adv. Drug Deliv. Rev.* **106**, 193–195 (2016). doi:10.1016/j.addr.2016.10.005 Medline

9. C. Prego, D. Torres, M. J. Alonso, The potential of chitosan for the oral administration of peptides. *Expert Opin. Drug Deliv.* **2**, 843–854 (2005). doi:10.1517/17425247.2.5.843 Medline

10. E. Mathiowitz, J. S. Jacob, Y. S. Jong, G. P. Carino, D. E. Chickering, P. Chaturvedi, C. A. Santos, K. Vijayaraghavan, S. Montgomery, M. Bassett, C. Morrell, Biologically erodable microspheres as potential oral drug delivery systems. *Nature* **386**, 410–414 (1997). doi:10.1038/386410a0 Medline

11. A. Banerjee, J. Wong, R. Gogoi, T. Brown, S. Mitragotri, Intestinal micropatches for oral insulin delivery. *J. Drug Target.* **25**, 608–615 (2017). doi:10.1080/1061186X.2017.1300664 Medline

12. M. C. Koetting, J. F. Guido, M. Gupta, A. Zhang, N. A. Peppas, pH-responsive and enzymatically-responsive hydrogel microparticles for the oral delivery of therapeutic proteins: Effects of protein size, crosslinking density, and hydrogel degradation on

protein delivery. *J. Control. Release* **221**, 18–25 (2016). doi:10.1016/j.jconrel.2015.11.023 Medline

13. C. B. Fox, Y. Cao, C. L. Nemeth, H. D. Chirra, R. W. Chevalier, A. M. Xu, N. A. Melosh, T. A. Desai, Fabrication of Sealed Nanostraw Microdevices for Oral Drug Delivery. *ACS Nano* **10**, 5873–5881 (2016). doi:10.1021/acsnano.6b00809 Medline

14. M. Davies, T. R. Pieber, M.-L. Hartoft-Nielsen, O. K. H. Hansen, S. Jabbour, J. Rosenstock, Effect of Oral Semaglutide Compared With Placebo and Subcutaneous Semaglutide on Glycemic Control in Patients With Type 2 Diabetes: A Randomized Clinical Trial. *JAMA* **318**, 1460–1470 (2017). doi:10.1001/jama.2017.14752 Medline

15. A. Banerjee, K. Ibsen, T. Brown, R. Chen, C. Agatemor, S. Mitragotri, Ionic liquids for oral insulin delivery. *Proc. Natl. Acad. Sci. U.S.A.* **115**, 7296–7301 (2018). doi:10.1073/pnas.1722338115 Medline

16. G. J. Tortora, B. H. Derrickson, *Principles of Anatomy and Physiology* (Wiley, ed. 12, 2008).

17. D. K. Podolsky, Healing the epithelium: Solving the problem from two sides. *J. Gastroenterol.* **32**, 122–126 (1997). doi:10.1007/BF01213309 Medline

18. J. L. Wallace, D. N. Granger, The cellular and molecular basis of gastric mucosal defense. *FASEB J.* **10**, 731–740 (1996). doi:10.1096/fasebj.10.7.8635690 Medline

19. I. P. Vazharov, Perforation as a complication of the diagnostic upper and lower endoscopy of the gastrointestinal tract. *J. IMAB* **18**, 273–275 (2012). doi:10.5272/jimab.2012183.273

20. G. M. Eisen, T. H. Baron, J. A. Dominitz, D. O. Faigel, J. L. Goldstein, J. F. Johanson, J. S. Mallery, H. M. Raddawi, J. J. Vargo 2nd, J. P. Waring, R. D. Fanelli, J. Wheeler-Harbough; American Society for Gastrointestinal Endoscopy, Complications of upper GI endoscopy. *Gastrointest. Endosc.* **55**, 784–793 (2002). doi:10.1016/S0016-5107(02)70404-5 Medline

21. L. Bolondi, M. Bortolotti, V. Santi, T. Calletti, S. Gaiani, G. Labò, Measurement of gastric emptying time by real-time ultrasonography. *Gastroenterology* **89**, 752–759 (1985). doi:10.1016/0016-5085(85)90569-4 Medline

22. G. Traverso, C. M. Schoellhammer, A. Schroeder, R. Maa, G. Y. Lauwers, B. E. Polat, D. G. Anderson, D. Blankschtein, R. Langer, Microneedles for drug delivery via the gastrointestinal tract. *J. Pharm. Sci.* **104**, 362–367 (2015). doi:10.1002/jps.24182 Medline

23. M. Imran, Therapeutic agent preparations for delivery into a lumen of the intestinal tract using a swallowable drug delivery device, U.S. Patent 9,844,655 (2017).

24. D. M. Bass, M. Prevo, D. S. Waxman, Gastrointestinal safety of an extended-release, nondeformable, oral dosage form (OROS): A retrospective study. *Drug Saf.* **25**, 1021–1033 (2002). doi:10.2165/00002018-200225140-00004 Medline

25. G. Domokos, P. L. Várkonyi, Geometry and self-righting of turtles. *Proc. Biol. Sci.* **275**, 11–17 (2008). doi:10.1098/rspb.2007.1188 Medline

26. P. L. Várkonyi, G. Domokos, Mono-monostatic bodies: The answer to Arnold's question. *Math. Intell.* **28**, 34–38 (2006). doi:10.1007/BF02984701

27. T. Santonen, H. Stockmann-Juvala, A. Zitting, *Review on Toxicity of Stainless Steel* (Finnish Institute of Occupational Health, 2010).

28. A. J. Ortiz, E. Fernández, A. Vicente, J. L. Calvo, C. Ortiz, Metallic ions released from stainless steel, nickel-free, and titanium orthodontic alloys: Toxicity and DNA damage. *Am. J. Orthod. Dentofacial Orthop.* **140**, e115–e122 (2011). doi:10.1016/j.ajodo.2011.02.021 Medline

29. M. Wang, L. Hu, C. Xu, Recent advances in the design of polymeric microneedles for transdermal drug delivery and biosensing. *Lab Chip* **17**, 1373–1387 (2017). doi:10.1039/C7LC00016B Medline

30. J. E. McKenzie, D. W. Osgood, Validation of a new telemetric core temperature monitor. *J. Therm. Biol.* **29**, 605–611 (2004). doi:10.1016/j.jtherbio.2004.08.020

31. G. Iddan, G. Meron, A. Glukhovsky, P. Swain, Wireless capsule endoscopy. *Nature* **405**, 417 (2000). doi:10.1038/35013140 Medline

32. D. Mikiewicz, A. Bierczyńska-Krzysik, A. Sobolewska, D. Stadnik, M. Bogiel, M. Pawłowska, A. Wójtowicz-Krawiec, P. A. Baran, N. Łukasiewicz, A. Romanik-Chruścielewska, I. Sokołowska, J. Stadnik, P. Borowicz, G. Płucienniczak, A. Płucienniczak, Soluble insulin analogs combining rapid- and long-acting hypoglycemic properties - From an efficient *E. coli* expression system to a pharmaceutical formulation. *PLOS ONE* **12**, e0172600 (2017). doi:10.1371/journal.pone.0172600 Medline

33. T. Glendorf, A. R. Sørensen, E. Nishimura, I. Pettersson, T. Kjeldsen, Importance of the solvent-exposed residues of the insulin B chain α-helix for receptor binding. *Biochemistry* **47**, 4743–4751 (2008). doi:10.1021/bi800054z Medline

34. T. N. Vinther, M. Norrman, U. Ribel, K. Huus, M. Schlein, D. B. Steensgaard, T. Å. Pedersen, I. Pettersson, S. Ludvigsen, T. Kjeldsen, K. J. Jensen, F. Hubálek, Insulin analog with additional disulfide bond has increased stability and preserved activity. *Protein Sci.* **22**, 296–305 (2013). doi:10.1002/pro.2211 Medline

35. C. Ortiz, D. Zhang, Y. Xie, V. J. Davisson, D. Ben-Amotz, Identification of insulin variants using Raman spectroscopy. *Anal. Biochem.* **332**, 245–252 (2004). doi:10.1016/j.ab.2004.06.013 Medline

36. M. J. Ferrua, R. P. Singh, Modeling the fluid dynamics in a human stomach to gain insight of food digestion. *J. Food Sci.* **75**, R151–R162 (2010). doi:10.1111/j.1750-3841.2010.01748.x Medline

37. N. Aoyagi, H. Ogata, N. Kaniwa, M. Uchiyama, Y. Yasuda, Y. Tanioka, Gastric emptying of tablets and granules in humans, dogs, pigs, and stomach-emptying-controlled rabbits. *J. Pharm. Sci.* **81**, 1170–1174 (1992). doi:10.1002/jps.2600811208 Medline